

Two-component scalar dark matter in Z_{2n} scenarios

Carlos E. Yaguna¹ and Óscar Zapata²

¹*Escuela de Física, Universidad Pedagógica y Tecnológica de Colombia,
Avenida Central del Norte # 39-115, Tunja, Colombia*

²*Instituto de Física, Universidad de Antioquia,
Calle 70 # 52-21, Apartado Aéreo 1226, Medellín, Colombia*

In multi-component scalar dark matter scenarios, a single Z_N ($N \geq 4$) symmetry may account for the stability of different dark matter particles. Here we study the case where N is even ($N = 2n$) and two species, a complex scalar and a real scalar, contribute to the observed dark matter density. We perform a phenomenological analysis of three scenarios based on the Z_4 and Z_6 symmetries, characterizing their viable parameter spaces and analyzing their detection prospects. Our results show that, thanks to the new interactions allowed by the Z_{2n} symmetry, current experimental constraints can be satisfied over a wider range of dark matter masses, and that these scenarios may lead to observable signals in direct detection experiments. Finally, we argue that these three scenarios serve as prototypes for other two-component Z_{2n} models with one complex and one real dark matter particle.

I. INTRODUCTION

Among the long series of models that have been proposed to explain the dark matter, the scalar singlet model [1–3] constitutes the simplest realization where a single particle lying around the electroweak scale has the suitable self-annihilation rate to achieve the observed dark matter abundance. Nevertheless, it is severely constrained by current observations. The dark matter mass must lie, in fact, either at the Higgs-resonance or above the TeV scale [4, 5]. Appealing alternatives to this paradigm are multi-component dark matter scenarios featuring scalar singlet fields that are stabilized by a single Z_N ($N \geq 4$) symmetry [6–9]¹.

The recent phenomenological study of the Z_5 -invariant two-component dark matter model [24], for instance, revealed that the dark matter masses may actually lie below the TeV while being consistent with current experimental bounds, and that both dark matter particles may give rise to observable signals in ongoing and forthcoming direct dark matter detection experiments. This Z_5 model, in addition, serves as a prototype for all the two-component scenarios based on a Z_N symmetry where the dark matter particles are both complex scalars. In this paper we will focus

¹ See Refs. [10–23] for pioneering studies on multi-component dark matter scenarios.

instead on models where the dark matter consists of a complex scalar and a real scalar.

This type of two-component scalar dark matter arises when N is even and one of the fields transforms as $\phi \rightarrow -\phi$ under the Z_N . In this work we explicitly consider the models based on the Z_4 and Z_6 symmetries. The latter admits two different charge assignments for the dark matter fields, one of them featuring unconditional stability [9] –an unusual property among Z_N models. For these three scenarios we perform a phenomenological analysis with the aim of identifying and characterizing the viable parameter space. Notably, we find that the dark matter masses may lie below the TeV and that the predicted direct detection rates can be within the expected sensitivity of future experiments [25, 26]. This new class of two-component dark matter models is thus shown to be not only theoretically compelling and phenomenologically consistent, but also experimentally testable.

The rest of the paper is organized as follows. In Section II we present a general discussion of two-component dark matter scenarios under a Z_{2n} symmetry, and introduce the Z_4 and Z_6 models that are the focus of our analysis. The phenomenological analysis is presented in III, where the viable parameter space of each scenario is established and illustrated, along with its detection prospects. A possible extension of these scenarios is introduced in Section IV while a generalization of our results to other Z_{2n} symmetries is sketched in Section V. Finally, in Section VI we draw our conclusions.

II. Z_{2n} MODELS

The two-component dark matter scenarios based on a Z_N symmetry extend the Standard Model (SM) with two scalar fields, ϕ_A and ϕ_B , that are SM singlets and have different Z_N charges, w_A and w_B respectively². If N is odd, these fields are necessarily complex and they both contribute to the observed dark matter density. The phenomenology of these scenarios was studied in detail in Ref. [24]. Here, we will focus instead in the case where N is even and one of the fields –say ϕ_B – is real with a charge $w_B = w^{N/2} = -1$, since $w = e^{i2\pi/N}$. Consequently, in these scenarios the dark matter consists of a complex scalar field (ϕ_A) and a real scalar field (ϕ_B).

Let us consider the most general scalar potential invariant under a Z_{2n} symmetry for two scalar singlets, one complex and one real, with ϕ_B having a Z_{2n} charge $w^n = -1$. The corresponding

² Two-component scenarios with scalar singlets (doublets) stabilized by two Z_2 or Z_3 symmetries have been studied in Refs. [27–31] ([32]).

potential can be written as the sum of two contributions,

$$\mathcal{V}_{Z_{2n}}(\phi_A, \phi_B) = \mathcal{V}_1(\phi_A, \phi_B) + \mathcal{V}_2(\phi_A, \phi_B). \quad (1)$$

The first one corresponds to the terms that are invariant for any Z_{2n} symmetry,

$$\begin{aligned} \mathcal{V}_1(\phi_A, \phi_B) \equiv & \mu_H^2 |H|^2 + \lambda_H |H|^4 + \mu_A^2 |\phi_A|^2 + \lambda_{4A} |\phi_A|^4 + \frac{1}{2} \mu_B^2 \phi_B^2 + \lambda_{4B} \phi_B^4 \\ & + \lambda_{4AB} |\phi_A|^2 \phi_B^2 + \lambda_{SA} |H|^2 |\phi_A|^2 + \frac{1}{2} \lambda_{SB} |H|^2 \phi_B^2, \end{aligned} \quad (2)$$

where H is the SM Higgs doublet. All the parameters appearing in \mathcal{V}_1 are real.

The interactions present in \mathcal{V}_1 may affect the dark matter phenomenology of these scenarios in different ways. The quartic interaction λ_{4AB} , for instance, induces dark matter conversion processes, while the λ_{Si} terms lead to $\phi_i \phi_i$ annihilations and to trilinear interactions between the dark matter particles and the Higgs. These interactions are crucial because they determine the elastic scattering of the dark matter particles off nuclei, providing a way to test these models via direct detection experiments. Notice that these models are particular realizations of the Higgs portal scenarios [33, 34], and natural extensions of the singlet scalar model [1–3].

The expression for the spin-independent (SI) cross-section is exactly the same as in the singlet scalar (or Higgs-portal) model and reads

$$\sigma_{\phi_i}^{\text{SI}} = \frac{\lambda_{Si}^2}{4\pi} \frac{\mu_R^2 m_p^2 f_p^2}{m_h^4 M_{\phi_i}^2}, \quad (3)$$

where μ_R is the reduced mass, m_p the proton mass, $f_p \approx 0.3$ is the quark content of the proton, and $M_{\phi_i}^2 = \mu_i^2 + \frac{1}{2} \lambda_{Si} v_H^2$ is the mass of the dark matter particle.

The second contribution to the scalar potential, \mathcal{V}_2 , contains the terms that are invariant for the specific Z_{2n} symmetry under consideration and for the given set of scalar fields, depending on their charges. Next we will examine \mathcal{V}_2 for the simplest realizations of these scenarios –those based on the Z_4 and Z_6 symmetries.

A. Z_4 model

In the Z_4 model the two scalar fields transform as

$$\phi_1 \sim \omega_4, \quad \phi_2 \sim \omega_4^2, \quad (4)$$

with $\omega_4 = \exp(i2\pi/4)$ and ϕ_2 playing the role of ϕ_B in the previous section. The \mathcal{V}_2 part of the scalar potential is

$$\mathcal{V}_2^{Z_4}(\phi_1, \phi_2) = \frac{1}{2} [\mu_{S1} \phi_1^2 \phi_2 + \lambda_{51} \phi_1^4] + \text{h.c.}, \quad (5)$$

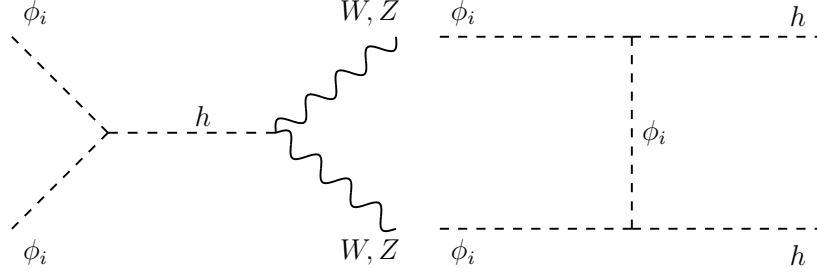


FIG. 1. Dark matter ϕ_i annihilation processes involving the λ_{S_i} interactions. These processes are common to both Z_4 and Z_6 models.

ϕ_1 Processes	Type	ϕ_2 Processes	Type
$\phi_1 + \phi_1^\dagger \rightarrow SM + SM$	1100	$\phi_2 + \phi_2 \rightarrow SM + SM$	2200
$\phi_1 + \phi_1^\dagger \rightarrow \phi_2 + \phi_2$	1122	$\phi_2 + \phi_2 \rightarrow \phi_1 + \phi_1^\dagger$	2211
$\phi_1 + \phi_1 \rightarrow \phi_2 + h$	1120	$\phi_2 + \phi_1 \rightarrow \phi_1^\dagger + h$	2110
		$\phi_2 + h \rightarrow \phi_1 + \phi_1$	2011

TABLE I. The $2 \rightarrow 2$ processes that are allowed in the Z_4 model and that can modify the relic density of ϕ_1 (left) and ϕ_2 (right). h denotes the SM Higgs boson. Conjugate and inverse processes are not shown.

which includes trilinear and quartic interactions among the new fields. The latter is a self-interaction term that plays no role in the present phenomenological study. The former, on the contrary, would render ϕ_2 unstable via the two-body decay $\phi_2 \rightarrow \phi_1 + \phi_1$. To obtain a two-component dark matter scenario it becomes necessary, therefore, to require $M_{\phi_2} < 2M_{\phi_1}$ so that ϕ_2 remains stable and contributes to the dark matter density. From now on this condition is assumed to be satisfied. The trilinear term, then, leads to dark matter conversion processes, and the interplay with the λ_{S1} and λ_{S2} interactions gives rise to the semi-annihilation processes showed in Fig. 2. As we will see in the next section, semi-annihilations play a major role in this model, allowing for a wider range of viable dark matter masses. Notice that the processes in the top panels modify the ϕ_2 number density by one unit whereas those in the bottom panels change the ϕ_1 number density by two units and the ϕ_2 number density by one unit.

The different processes that contribute to the relic densities of ϕ_1 and ϕ_2 are shown in table I, classified according to their type. The Boltzmann equations for the Z_4 model thus read

$$\frac{dn_1}{dt} = -\sigma_v^{1100} (n_1^2 - \bar{n}_1^2) - \sigma_v^{1120} \left(n_1^2 - n_2 \frac{\bar{n}_1^2}{\bar{n}_2} \right) - \sigma_v^{1122} \left(n_1^2 - n_2^2 \frac{\bar{n}_1^2}{\bar{n}_2^2} \right) - 3Hn_1, \quad (6)$$

$$\frac{dn_2}{dt} = -\sigma_v^{2200} (n_2^2 - \bar{n}_2^2) - \sigma_v^{2211} \left(n_2^2 - n_1^2 \frac{\bar{n}_2^2}{\bar{n}_1^2} \right) - \frac{1}{2}\sigma_v^{1210} (n_1n_2 - n_1\bar{n}_2) + \frac{1}{2}\sigma_v^{1120} (n_1^2 - n_2 \frac{\bar{n}_1^2}{\bar{n}_2}) - 3Hn_2. \quad (7)$$

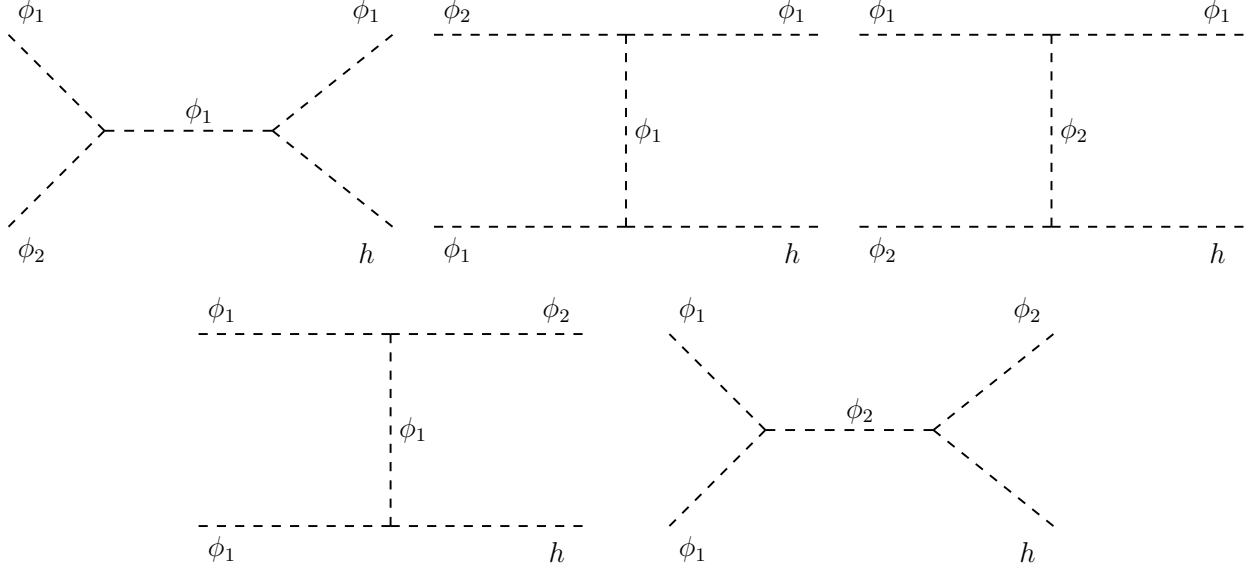


FIG. 2. Semi-annihilation processes in the Z_4 model, which are generated by the μ_{S1} interaction along with one Higgs portal interaction.

Here σ_v^{abcd} stands for the thermally averaged cross section, which satisfies

$$\bar{n}_a \bar{n}_b \sigma_v^{abcd} = \bar{n}_c \bar{n}_d \sigma_v^{cdab}. \quad (8)$$

whereas n_i ($i = 1, 2$) denote the number densities of ϕ_i , and \bar{n}_i their respective equilibrium values. To numerically solve these equations and obtain the relic densities we use **micrOMEGAs** [22] throughout this paper. Since its version 4.1, **micrOMEGAs** incorporates two-component dark matter scenarios, automatically including all the relevant processes in a given model.

Even though the free parameters in the \mathcal{V}_2 potentials are in principle complex, taking them to be real is not expected to modify in any significant way the results. For simplicity, in the following it is assumed that they are real.

B. Z_6 model

For the Z_6 model there are two possible charge assignments

$$\phi_1 \sim \omega_6, \quad \phi_3 \sim \omega_6^3, \quad \text{or} \quad \phi_2 \sim \omega_6^2, \quad \phi_3 \sim \omega_6^3, \quad (9)$$

with $\omega_6 = \exp(i\pi/3)$ and ϕ_3 playing the role of ϕ_B in the previous section. Thus, two distinct scenarios arise, which we denote as $Z_6(13)$ and $Z_6(23)$ respectively. The scalar potential \mathcal{V}_2 for the $Z_6(13)$ scenario turns out to be

$$\mathcal{V}_2^{Z_6}(\phi_1, \phi_3) = \frac{1}{3} \lambda'_{41} \phi_1^3 \phi_3 + \text{h.c.}, \quad (10)$$

ϕ_1 Processes	Type	ϕ_3 Processes	Type
$\phi_1 + \phi_1^\dagger \rightarrow SM + SM$	1100	$\phi_3 + \phi_3 \rightarrow SM + SM$	3300
$\phi_1 + \phi_1^\dagger \rightarrow \phi_3 + \phi_3$	1133	$\phi_3 + \phi_3 \rightarrow \phi_1 + \phi_1^\dagger$	3311
$\phi_1 + \phi_1 \rightarrow \phi_3 + \phi_1^\dagger$	1131	$\phi_3 + \phi_1 \rightarrow \phi_1^\dagger + \phi_1^\dagger$	3111

TABLE II. The $2 \rightarrow 2$ processes that are allowed in the $Z_6(13)$ model and that can modify the relic density of ϕ_1 (left) and ϕ_3 (right). Notice that semi-annihilation processes are not allowed in this model. Conjugate and inverse processes are not shown.

ϕ_2 Processes	Type	ϕ_3 Processes	Type
$\phi_2 + \phi_2^\dagger \rightarrow SM + SM$	2200	$\phi_3 + \phi_3 \rightarrow SM + SM$	3300
$\phi_2 + \phi_2^\dagger \rightarrow \phi_3 + \phi_3$	2233	$\phi_3 + \phi_3 \rightarrow \phi_2 + \phi_2^\dagger$	3322
$\phi_2 + \phi_2 \rightarrow \phi_2^\dagger + h$	2220		

TABLE III. The $2 \rightarrow 2$ processes that are allowed in the $Z_6(23)$ model and that can modify the relic density of ϕ_1 (left) and ϕ_3 (right). h denotes the SM Higgs boson. Conjugate and inverse processes are not shown.

and includes only quartic interactions. To guarantee that ϕ_3 is stable, the condition $M_{\phi_3} < 3M_{\phi_1}$ is assumed to hold in the following. Due to the absence of trilinear interactions, there are no semi-annihilation processes in this case. The λ'_{41} interaction gives rise to dark matter conversion processes only. The processes that affect the relic density are displayed in table II. From them, the Boltzmann equations can be written down.

For the $Z_6(23)$ scenario, \mathcal{V}_2 reads

$$\mathcal{V}_2^{Z_6}(\phi_2, \phi_3) = \frac{1}{3}\mu_{32}\phi_2^3 + \text{h.c.} \quad (11)$$

Since there are neither cubic nor quartic terms involving one single field, ϕ_2 and ϕ_3 are both stable independently of their masses –an unusual situation dubbed *unconditional stability* [9]. The Z_6 symmetry with ϕ_2 and ϕ_3 is, in fact, the simplest realization of unconditional stability for two dark matter particles³. The cubic self-interaction term μ_{32} in Eq. (11) along with the λ_{S2} interaction give rise to semi-annihilation processes affecting only the number of ϕ_2 particles (see Figure 3), which, in the next section, will be shown to be quite important. Table III shows the processes that must be taken into account in the Boltzmann equations for this model.

This $Z_6(23)$ scenario can be seen as a two-component extension of the Z_3 scalar singlet model [35–37], for it includes all the terms present in it. Recently, a $U(1)$ extension of this scenario was

³ Notice that unconditional stability is not limited to the renormalizable Lagrangian but is maintained for operators of arbitrary dimension.

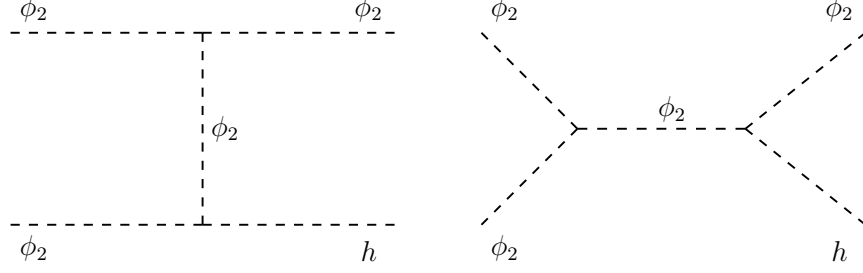


FIG. 3. Semi-annihilation processes in the $Z_6(23)$ scenario governed by the trilinear self-interaction μ_{32} and the Higgs portal λ_{52} .

studied in Ref. [38], which reaffirms one of the main theoretical advantages of Z_N models: they can be easily incorporated into gauge extensions of the Standard Model.

III. THE VIABLE PARAMETER SPACE

Here we will obtain and study viable regions of the Z_4 and Z_6 models described in the previous section. To that end, the parameter space will be randomly scanned and the points compatible with the constraints obtained from the invisible decays of the Higgs boson, dark matter density [39] and direct dark matter searches [40] will be selected. This sample of viable points will then be analyzed, paying particular attention to the dark matter detection prospects. Let us stress that this random sampling of the parameter space does not allow a statistical interpretation of the distribution of viable points—it cannot be used to identify the best fit point or the most favored regions. It should be enough, however, for our purposes: to find the most relevant parameters and to identify the mechanisms that allow to satisfy the current bounds.

If the dark matter particles are lighter than half the Higgs mass, the decay $h \rightarrow \phi_i^* \phi_i$ would be allowed, contributing to the invisible branching ratio of the Higgs boson (\mathcal{B}_{inv}). The decay width associated with $h \rightarrow \phi_i^* \phi_i$ is

$$\Gamma(h \rightarrow \phi_i^* \phi_i) = \eta_{\phi_i} \frac{\lambda_{Si}^2 v_H^2}{32\pi M_h} \left[1 - \frac{4M_{\phi_i}^2}{M_h^2} \right]^{1/2}, \quad (12)$$

where $\eta_{\phi_i} = 1(2)$ for ϕ_i real (complex). To be consistent with current data, we require that $\mathcal{B}_{inv} \leq 0.13$) [41, 42].

The relic density constraint reads

$$\Omega_{\phi_A} + \Omega_{\phi_B} = \Omega_{\text{DM}}, \quad (13)$$

where Ω_{DM} is the dark matter abundance as reported by PLANCK [39],

$$\Omega_{\text{DM}} h^2 = 0.1198 \pm 0.0012. \quad (14)$$

We consider a model to be consistent with this measurement if its relic density, as computed by micrOMEGAs, lies between 0.11 and 0.13, which takes into account an estimated theoretical uncertainty of order 10%. Since we have two dark matter particles, an important quantity in our analysis is the fractional contribution of each to the total dark matter density, $\xi_{\phi_i} \equiv \Omega_{\phi_i}/\Omega_{\text{DM}}$, with $\xi_{\phi_A} + \xi_{\phi_B} = 1$.

In our study, we require the spin-independent cross section, computed from equation (3), to be below the direct detection limit set by the XENON1T collaboration [40]. Such direct detection limit usually provides very strong constraints on Higgs-portal scenarios like the models we are discussing. In particular, for the singlet real scalar model [1–3] the minimum dark matter mass compatible with upper limit set by the XENON1T collaboration is ~ 950 GeV (for the complex case turns to be ~ 2 TeV). As we will show, however, the new interactions present in the Z_4 and Z_6 scenarios allow us to simultaneously satisfy the relic density constraint and direct detection limits for lower dark matter masses.

In addition, we will study the testability of the viable models at future direct detection experiments including LZ [25] and DARWIN [26], as well as the possible constraints from indirect detection searches. For these searches, the relevant particle physics quantity is no longer $\langle\sigma v\rangle$ but $\xi_i \xi_j \langle\sigma v\rangle_{ij}$, where $\langle\sigma v\rangle_{ij}$ is the cross section times velocity for the annihilation process of dark matter particles i and j into a certain final state. The computation of the different annihilation rates is performed with the help of micrOMEGAS. We will rely on the limits and on the projected sensitivities reported by the Fermi collaboration from γ -ray observations of dShps [43, 44].

We have performed several random scans, varying just a subset of the free parameters of the model at a time so as to make the analysis simpler. In all the scans, the dark matter masses and the Higgs-portal couplings are randomly sampled (using a logarithmically-uniform distribution) in the following ranges:

$$40 \text{ GeV} \leq M_{\phi_A}, M_{\phi_B} \leq 2 \text{ TeV}, \quad (15)$$

$$10^{-4} \leq |\lambda_{SA}|, |\lambda_{SB}| \leq 1. \quad (16)$$

The remaining parameters are crucial because they alleviate the strong correlation between the dark matter annihilations that set the relic density and the scattering off nuclei that are constrained by direct detection searches, probably allowing for viable models at low dark matter masses ($M_{\phi_i} \lesssim$

1 TeV). The Z_5 model [24], for instance, became viable over the entire dark matter mass range due to the trilinear interaction term $\phi_1^2\phi_2$. We expect, therefore, a similar situation in the Z_4 model and, up to a large extent, in the $Z_6(23)$ scenario. The dimensionful parameters, μ_{S1} and μ_{32} , will be varied (within each scenario) up to a maximum value (10 TeV), which is not far from the maximum value allowed for the heaviest dark matter particle (4 TeV).

A. Z_4 model

In this model the \mathcal{V}_2 potential contains the trilinear interaction $\phi_1^2\phi_2$ which induces semi-annihilation processes that may help decrease the number density of dark matter particles. The associated coupling is chosen as

$$100 \text{ GeV} \leq \mu_{S1} \leq 10 \text{ TeV}. \quad (17)$$

The remaining free parameter of the model, λ_{41} , is varied in the interval⁴

$$10^{-4} \leq |\lambda_{412}| \leq 1. \quad (18)$$

Both couplings were sampled using a log-uniform distribution in the given range. It is convenient to separately investigate the two possible mass hierarchies for the dark matter particles in this scenario $-M_{\phi_1} < M_{\phi_2}$ and $M_{\phi_2} < M_{\phi_1}$. The resulting viable parameter space is shown in figures 4 and 5, respectively. The most important conclusion that can be drawn from these figures is that, in contrast with the singlet scalar model, it is indeed possible to satisfy current bounds with dark matter masses below the TeV scale. In fact, the entire range of dark matter masses explored in the scan turns out to be viable.

From the top-left panel of figure 4 we see that ϕ_1 gives the dominant contribution to the dark matter density for most of the viable points in our scan, usually accounting for more than 90% of it. In fact, in multiple cases Ω_{ϕ_2} turns out to be several orders of magnitude smaller than Ω_{ϕ_1} . This hierarchy is a consequence of the new Z_4 interactions, which tend to suppress the relic density of the heavier particle more than that of the lighter one –because the former can annihilate into the latter.

The fact that semi-annihilation processes (see Fig. 2) are essential to obtain the correct relic density while satisfying direct detection bounds is illustrated in the top-right panel, which shows the trilinear coupling versus M_{ϕ_1} . Notice that the minimum value of μ_{S1} found in our sample increases

⁴ Notice that λ_{51} plays no role in the current analysis.

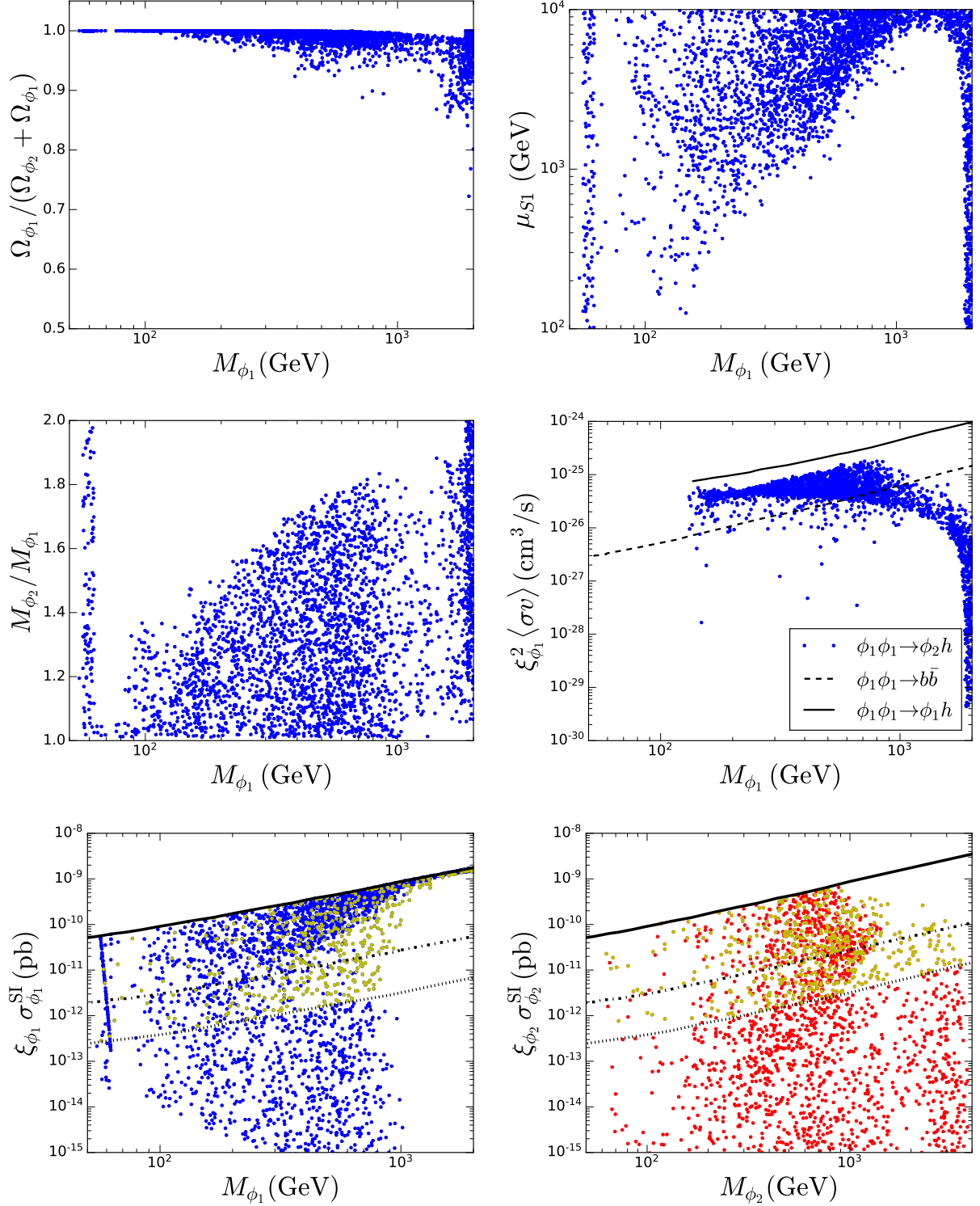


FIG. 4. A sample of viable points of the Z_4 model with $M_{\phi_1} < M_{\phi_2}$, projected along different dimensions. The top panels show scatter plots of M_{ϕ_1} versus $\Omega_{\phi_1}/\Omega_{DM}$ (left) and versus μ_{S1} (right). In the center panels, the ratio of dark matter masses (left) and the most relevant indirect detection signal (right) are illustrated. The direct detection prospects are shown in the bottom panels for ϕ_1 (left) and ϕ_2 (right).

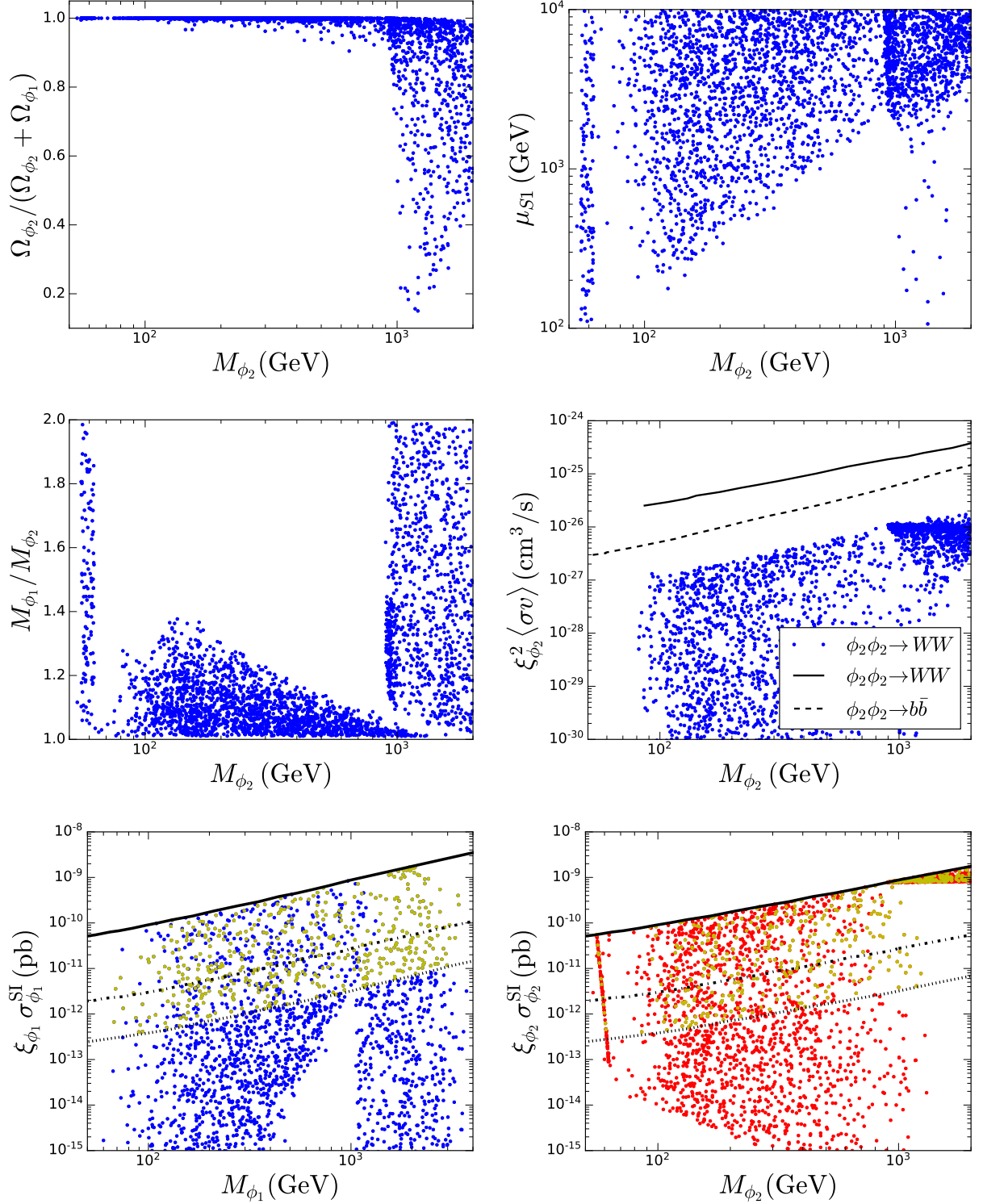


FIG. 5. A sample of viable points of the Z_4 model with $M_{\phi_2} < M_{\phi_1}$, projected along different dimensions. The top panels show scatter plots of M_{ϕ_2} versus $\Omega_{\phi_2}/\Omega_{DM}$ (left) and versus μ_{S1} (right). In the center panels, the ratio of dark matter masses (left) and the most relevant indirect detection signal (right) are illustrated. The direct detection prospects are shown in the bottom panels for ϕ_1 (left) and ϕ_2 (right).

with M_{ϕ_1} up to about 1 TeV, when it reaches the maximum value allowed in the scan (10 TeV). At $M_{\phi_1} \sim 2$ TeV or higher, the trilinear couplings can be small because the standard Higgs portal becomes consistent with current data. The center-left panel displays the ratio M_{ϕ_2}/M_{ϕ_1} , whose range of variation tends to increase with M_{ϕ_1} . This figure demonstrates that, in this scenario, the masses of the dark matter particles are not required to be degenerate.

Regarding indirect detection, the dominant annihilation channel in our sample turns out to be the semi-annihilation process $\phi_1 + \phi_1 \rightarrow \phi_2 + h$. Due to the Ω_{ϕ_2} suppression, all the ϕ_2 annihilation channels feature instead much lower rates. The center-right panel displays the $\phi_1 + \phi_1 \rightarrow \phi_2 + h$ rate versus M_{ϕ_1} for our sample of viable points. Since up to date there is no reported experimental limit on such a process, we show, for comparison purposes, the current limit on the related process $\phi_1 + \phi_1 \rightarrow \phi_1 + h$ (solid line) [45], which should be slightly stronger than the one on $\phi_1 + \phi_1 \rightarrow \phi_2 + h$. From the figure we conclude that none of the viable points found in our scan is excluded by the current limit. The dashed line corresponds instead to the projected sensitivity, assuming 45 dSphs and 15 years of observation [44], for the process $\phi_1 + \phi_1 \rightarrow b + \bar{b}$, which yields a higher γ -ray flux than $\phi_1 + \phi_1 \rightarrow \phi_2 + h$. It is unclear, therefore, whether future observations will be able to set constraints on the viable points of this scenario.

In the bottom panels, the direct detection rates for both dark matter particles are compared against the experimental results. The solid line shows the current limit from XENON1T, which is necessarily satisfied due to our selection procedure, while the dashed and dotted lines correspond to the expected sensitivities of LZ [25] and DARWIN [26] respectively. In this figures, the yellow points denote the viable models for which *both* dark matter particles are expected to yield signals in future direct detection experiments. From these two panels we conclude that either dark matter particle may be observed in future direct detection experiments, and that in several cases both dark matter particles might be observed.

The results for the case where $M_{\phi_2} < M_{\phi_1}$ (see Fig. 5) are qualitatively similar to those for $M_{\phi_1} < M_{\phi_2}$. The main difference is that in this case a mild degeneracy is required between the dark matter particles. In fact, notice from the center-left panel that M_{ϕ_2}/M_{ϕ_1} does not exceed 1.4 within our sample of viable points. It is worth mentioning that despite the fact that for values of M_{ϕ_2} above 950 GeV the Z_4 interactions are not compulsory to achieve a depletion on Ω_{ϕ_2} , they are still necessary to allow for efficient ϕ_1 self-annihilations. As can be seen from the center-right panel, the indirect detection prospects are not encouraging in this case. It shows the rate for the dominant annihilation channel in our sample, which happens to be $\phi_2 + \phi_2^\dagger \rightarrow W^+ W^-$, and compares it against the corresponding current limit reported by the Fermi collaboration [43] (solid

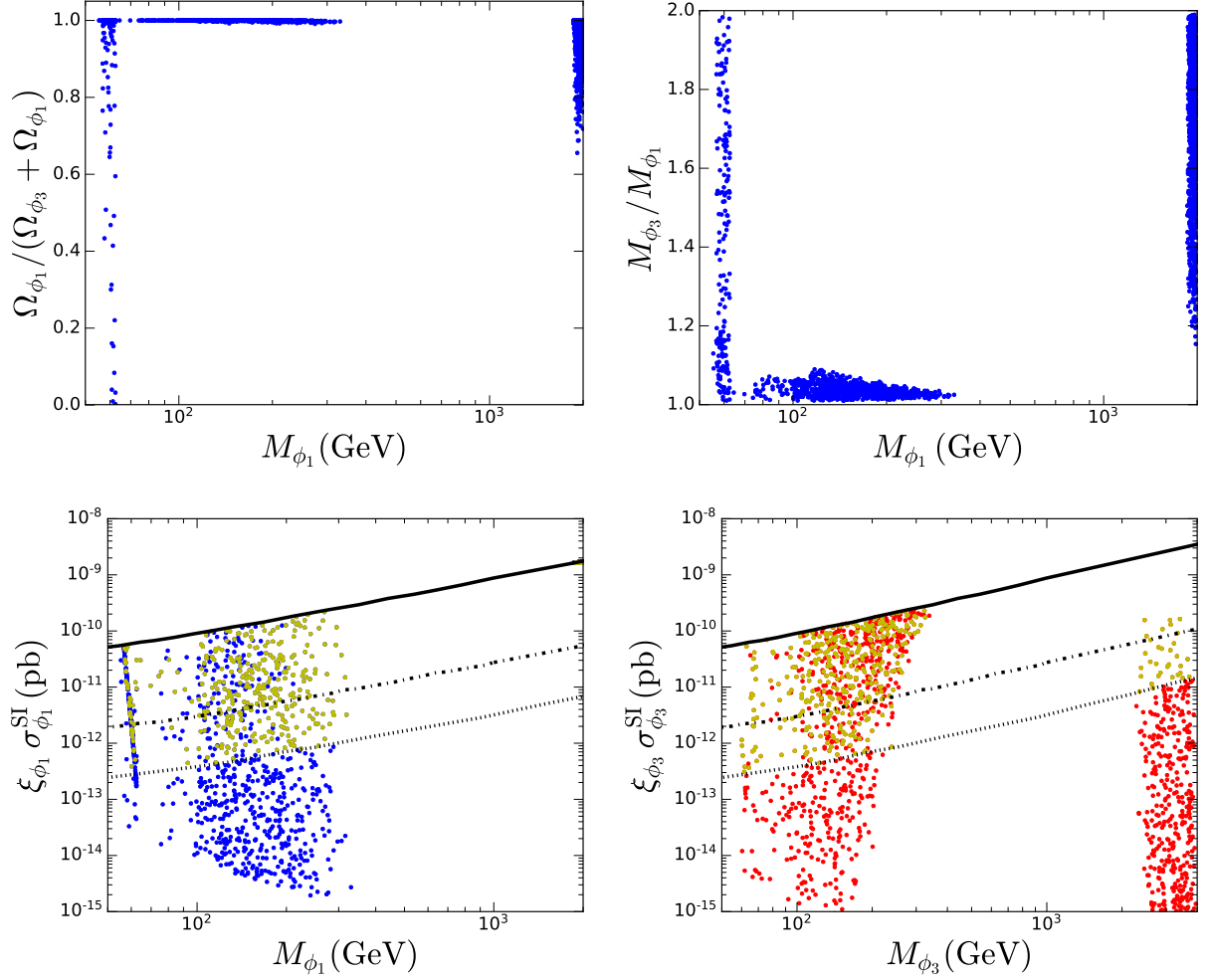


FIG. 6. A sample of viable points of the Z_6 model with (ϕ_1, ϕ_3) and $M_{\phi_1} < M_{\phi_3}$, projected along different dimensions. The top panels show scatter plots of M_{ϕ_1} versus $\Omega_{\phi_1}/\Omega_{DM}$ (left) and versus the ratio of dark matter masses (right). The direct detection prospects are shown in the bottom panels for ϕ_1 (left) and ϕ_3 (right).

line). All the viable points lie well below the current bound. Even future Fermi data (dashed line) will be unable to exclude viable points. Future direct detection experiments, on the other hand, will set significant constraints on this scenario (see bottom panels) and constitute the most promising way to test it.

Finally, our scans indicate that, independently of the mass hierarchy, the λ_{412} interaction does not play an essential role in setting the dark matter abundances. It is instead the trilinear couplings, via the semi-annihilation processes they induce, that modify the relic density and allow to have dark matter masses below a TeV.

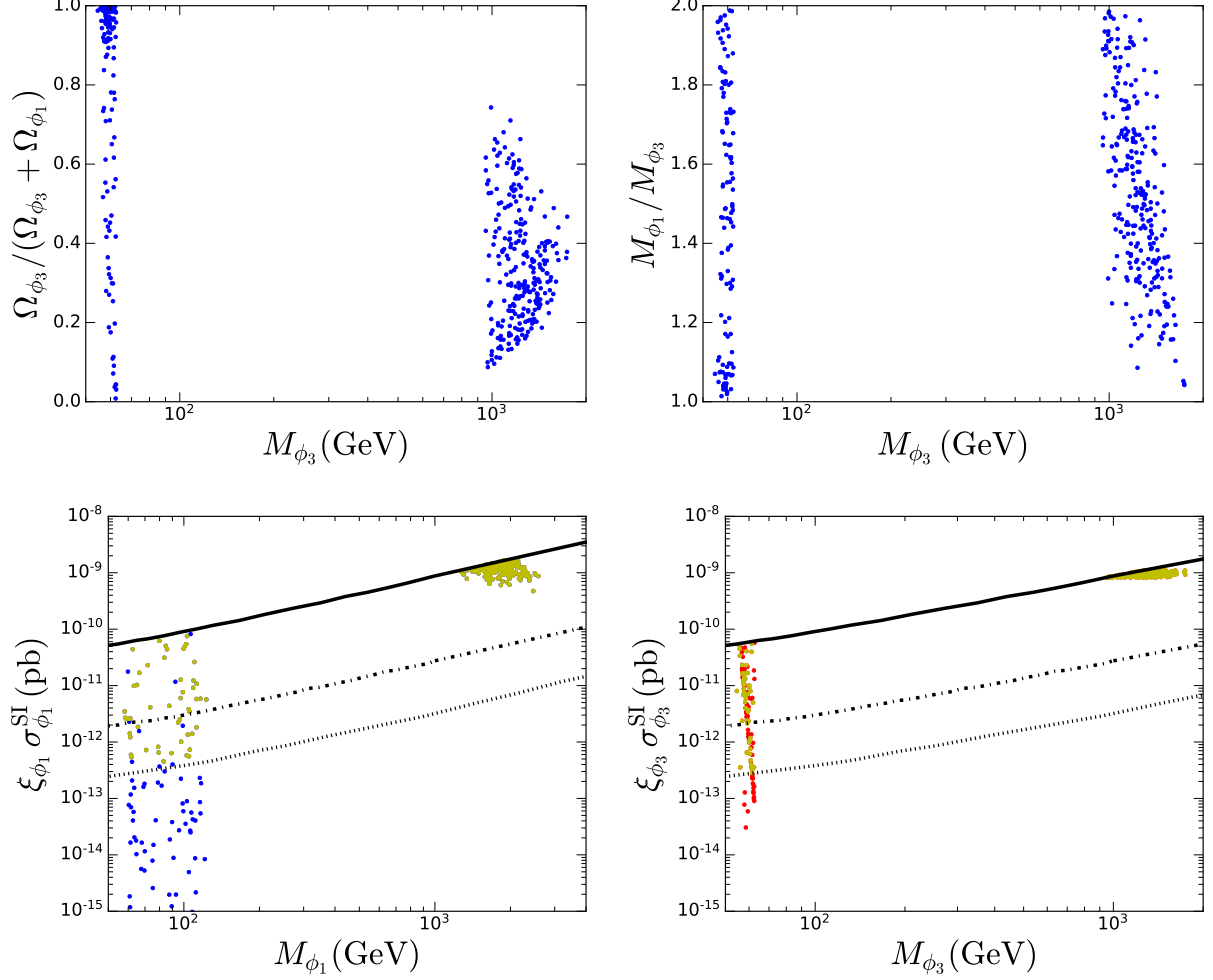


FIG. 7. A sample of viable points of the Z_6 model with (ϕ_1, ϕ_3) and $M_{\phi_3} < M_{\phi_1}$, projected along different dimensions. The top panels show scatter plots of M_{ϕ_1} versus $\Omega_{\phi_1}/\Omega_{DM}$ (left) and versus the ratio of dark matter masses (right). The direct detection prospects are shown in the bottom panels for ϕ_1 (left) and ϕ_3 (right).

B. $Z_6(13)$ model

The unique new interaction associated to this model is λ'_{41} (see Eq. (10)), which only generates dark matter conversion processes of the type $\phi_1 \leftrightarrow \phi_3$. In our scans λ_{413} and λ'_{41} are randomly sampled using a log-uniform distribution in the range

$$10^{-4} \leq |\lambda_{413}|, |\lambda'_{41}| \leq 1. \quad (19)$$

The results from the scan are displayed in figures 6 and 7 for the $M_{\phi_1} < M_{\phi_3}$ and $M_{\phi_3} < M_{\phi_1}$, respectively. In the former case, the main effect of the quartic interactions is to open up a new

viable region with $70 \text{ GeV} \lesssim M_{\phi_1} \lesssim 300 \text{ GeV}$ –the region between 300 and 1850 GeV features no viable points in our sample. And it is ϕ_1 , the lighter dark matter particle, that accounts for most of the relic density in the new viable region –see top right panel. In this case, the depletion of Ω_{ϕ_1} is rather inefficient because it proceeds via λ'_{41} -induced dark matter conversion processes, which are only possible when the dark matter particles are mass degenerate (so that the kinematic suppression is not that strong). In fact, notice from the top-right panel that the degree of degeneracy is always below 10% and decreases with M_{ϕ_1} . As was the case in the Z_4 model, the λ_{413} interaction plays no role here. Regarding detection prospects, the bottom panels show that a significant fraction of the viable points in our scan lies within the expected sensitivity of future experiments. Due to the mass degeneracy, however, it would be extremely difficult if not altogether impossible to disentangle the possible signals from the two dark matter particles.

For $M_{\phi_3} < M_{\phi_1}$, instead, there are no new viable points in our sample –the whole range of M_{ϕ_3} from 70 to 950 GeV appears excluded. The reason is that the process $\phi_1 + \phi_3 \rightarrow \phi_1 + \phi_1$, which reduces the ϕ_3 number density, is Boltzmann suppressed in this case. This example illustrates the fact that the new interactions allowed by the Z_{2n} symmetry not always succeed in opening up new regions of parameter space. In the next section, we will propose a simple extension of this scenario that succeeds in doing so.

C. $Z_6(23)$ model

The free parameters in this scenario are varied randomly using a logarithmic scan within the ranges

$$10^{-4} \leq |\lambda_{423}| \leq 1 \quad (20)$$

$$100 \text{ GeV} \leq \mu_{32} \leq 10 \text{ TeV}. \quad (21)$$

For $M_{\phi_2} < M_{\phi_3}$, the results of the scan are displayed in figure 8. Thanks to the semi-annihilation processes (see figure 3), the entire range above the higgs mass turns out to be viable for M_{ϕ_2} (and M_{ϕ_3}). For $M_{\phi_2} \lesssim 1 \text{ TeV}$, no preference is observed in our sample regarding the fraction of the dark matter contributed by each particle, but for $M_{\phi_2} \gtrsim 1 \text{ TeV}$, both particles tend to contribute significantly –see the top-left panel. In the top-right panel one can see that the minimum value of μ_{32} increases with M_{ϕ_2} , as expected for a semi-annihilation driven relic density. With respect to the ratio of the dark matter masses, the center panel shows that it varies over a wide range for the viable points we found, indicating that the dark matter particles are not required to be degenerate,

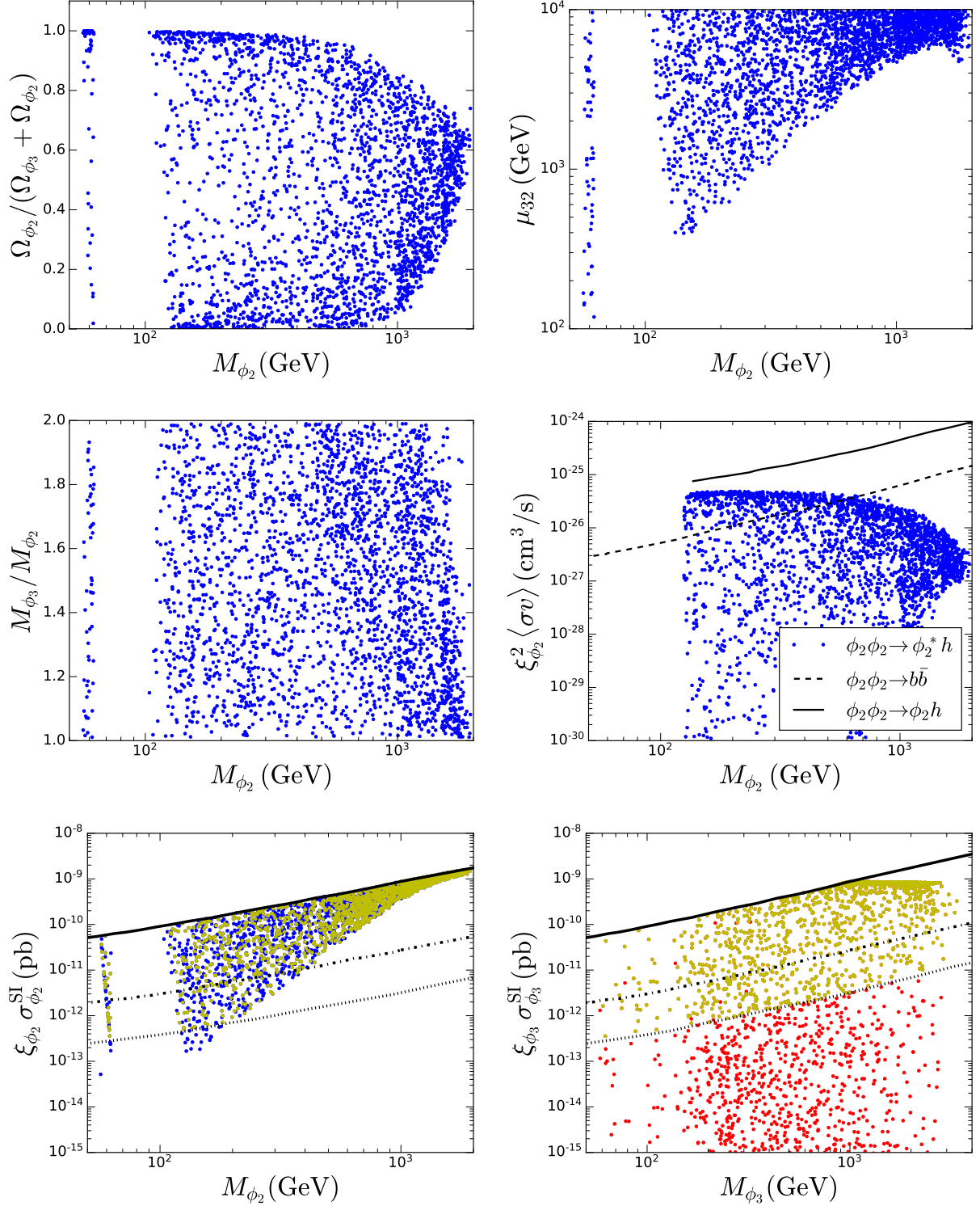


FIG. 8. A sample of viable points of the $Z_6(23)$ model with $M_{\phi_2} < M_{\phi_3}$, projected along different dimensions. The top panels show scatter plots of M_{ϕ_2} versus $\Omega_{\phi_2}/\Omega_{DM}$ (left) and versus μ_{32} (right). In the center panels, the ratio of dark matter masses (left) and the most relevant indirect detection signal (right) are illustrated. The direct detection prospects are shown in the bottom panels for ϕ_2 (left) and ϕ_3 (right).

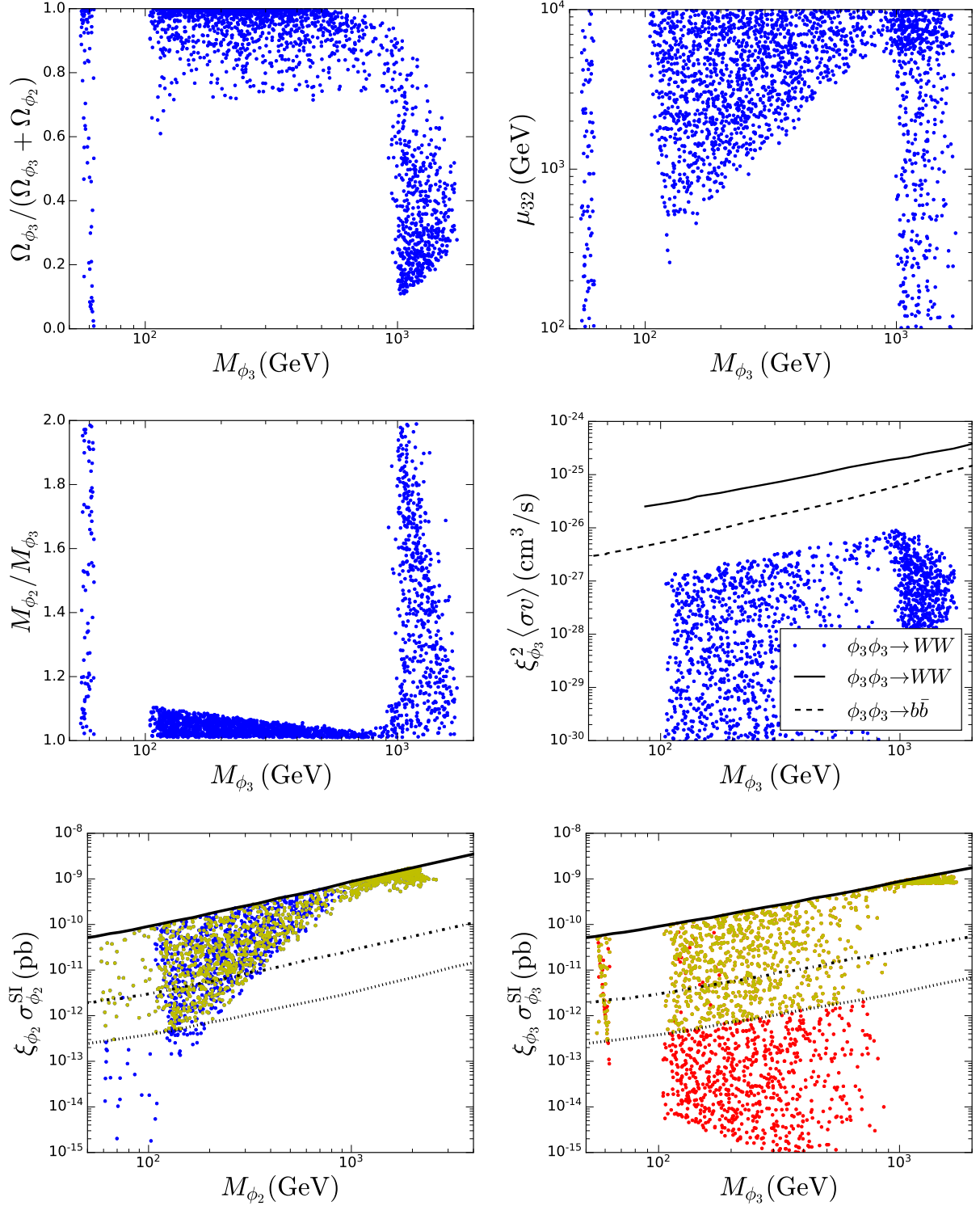


FIG. 9. A sample of viable points of the $Z_6(23)$ model with $M_{\phi_3} < M_{\phi_2}$, projected along different dimensions. The top panels show scatter plots of M_{ϕ_3} versus $\Omega_{\phi_3}/\Omega_{DM}$ (left) and versus μ_{32} (right). In the center panels, the ratio of dark matter masses (left) and the most relevant indirect detection signal (right) are illustrated. The direct detection prospects are shown in the bottom panels for ϕ_2 (left) and ϕ_3 (right).

in stark contrast with the $Z_6(13)$ model. The dominant dark matter annihilation channel in our sample happens to be the semi-annihilation process $\phi_2 + \phi_2 \rightarrow \phi_2^* + h$. And, as seen from the center-right panel, indirect detection does not currently constraint our set of viable models. A remarkable feature of this scenario is that the detection of ϕ_2 at DARWIN is practically guaranteed for all the points in our sample –only few points at low masses may evade detection in such an experiment (see bottom-left panel). Such an encouraging situation had not arisen in the previous scenarios we discussed.

For $M_{\phi_3} < M_{\phi_1}$, see figure 9, the range of M_{ϕ_3} with viable points goes up to 1700 GeV, where λ_{S_3} saturates the maximum value considered in our scan. The viable points below $M_{\phi_3} \lesssim 950$ GeV demand a strong mass degeneracy, namely $M_{\phi_2}/M_{\phi_3} \lesssim 1.1$ (see center panel), and a sizeable λ_{423} quartic coupling, $|\lambda_{423}| \gtrsim 0.1$. Indeed, the semi-annihilation processes generated by the μ_{32} interaction only affect the number density of the ϕ_2 , which means that ϕ_3 annihilates through the Higgs portal interactions or Boltzmann-suppressed conversion processes. The dominant annihilation channel in our sample is now $\phi_3 + \phi_3 \rightarrow WW$ but its rates are too small to be observed with current or future Fermi data –see center-right panel. The direct detection prospects, on the contrary, are seen to be similar to the previous case (see bottom panels), with an almost certain detection of ϕ_2 at DARWIN, but with the caveat that the dark matter particles are highly degenerate, implying that it will be challenging to distinguish this scenario from those with just one dark matter particle.

In this section we investigated the phenomenology of three scenarios for two-component dark matter based on the Z_4 and Z_6 symmetries. In all of them the dark matter consists of two scalars that are singlets under the SM gauge group –one of them is complex and the other is real. Our analysis reveals that, thanks to the new semi-annihilation and dark matter conversion processes that are allowed by the Z_{2n} symmetries, it is often possible to satisfy all the theoretical and experimental bounds over a wide range of dark matter masses, especially below 1 TeV. These models are also testable via current and forthcoming direct detection experiments, which may be able to detect signals from both dark matter particles.

IV. NON-MINIMAL MODELS

As we have seen in the previous section, in some cases the new Z_{2n} interactions are unable to open up new regions of viable parameter space. It is natural to ask, therefore, whether there is a simple way to extend such models and achieve that goal. A direct and rather trivial extension

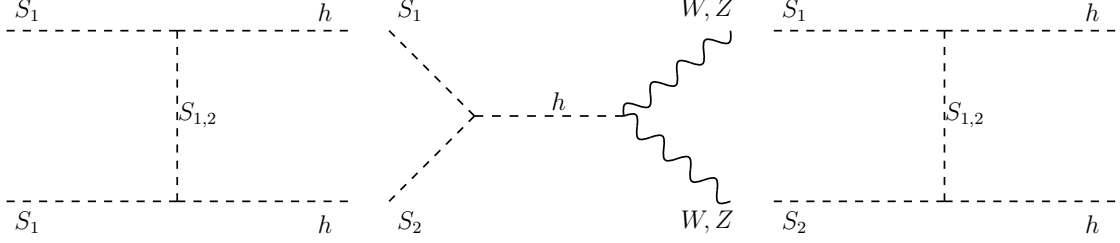


FIG. 10. Dark matter S_1 annihilation (left) and $S_1 - S_2$ coannihilation (center and right) processes involving the λ_6 and λ_{SB} interactions.

of the framework assumed so far is to consider ϕ_B as a complex field. In this section we analyze such a possibility. Let us stress that unlike ϕ_A , which is necessarily complex, ϕ_B may be real, but it does not have to be so. We will see that when ϕ_B is complex, it splits into two real fields, the lighter one being a dark matter particle (the other dark matter particle is ϕ_A). We call these models non-minimal because they contain an extra particle in the dark sector (the heavier one left from the splitting of ϕ_B) that is unstable and does not contribute to the dark matter.

Under the assumption that ϕ_B is complex the corresponding potential can be written as the sum of three contributions,

$$\mathcal{V}_{Z_{2n}}(\phi_A, \phi_B) = \mathcal{V}_1(\phi_A, \phi_B) + \mathcal{V}_2(\phi_A, \phi_B) + \mathcal{V}_3(\phi_A, \phi_B), \quad (22)$$

where the first and second contributions are analogous to the ones in the case of ϕ_B real. Concretely, for \mathcal{V}_1 we have

$$\begin{aligned} \mathcal{V}_1(\phi_A, \phi_B) \equiv & \mu_H^2 |H|^2 + \lambda_H |H|^4 + \mu_A^2 |\phi_A|^2 + \lambda_{4A} |\phi_A|^4 + \mu_B^2 |\phi_B|^2 + \lambda_{4B} |\phi_B|^4 \\ & + \lambda_{4AB} |\phi_A|^2 |\phi_B|^2 + \lambda_{SA} |H|^2 |\phi_B|^2 + \lambda_{SB} |H|^2 |\phi_B|^2. \end{aligned} \quad (23)$$

In the third contribution, the additional terms associated to the field ϕ_B that are invariant for any Z_{2n} symmetry are grouped. It can be written as

$$\mathcal{V}_3(\phi_A, \phi_B) \equiv \frac{1}{2} [\kappa^2 \phi_B^2 + \lambda_6 |H|^2 \phi_B^2 + \lambda_{5B} \phi_B^4 + \lambda'_{4AB} |\phi_A|^2 \phi_B^2 + \lambda'_{5B} |\phi_B|^2 \phi_B^2] + \text{h.c.} \quad (24)$$

After the electroweak symmetry breaking the real and imaginary components of $\phi_B = (\phi_{BR} + i\phi_{BI})/\sqrt{2}$ get mixed through the κ^2 and λ_6 terms in \mathcal{V}_3 . Specifically, the 2×2 mass matrix in the basis (ϕ_{BR}, ϕ_{BI}) has the entries

$$M_{11}^2 = \mu_B^2 + \Re(\kappa^2) + \frac{1}{2}(\lambda_{SB} + \Re(\lambda_6))v_H^2, \quad (25)$$

$$M_{22}^2 = \mu_B^2 - \Re(\kappa^2) + \frac{1}{2}(\lambda_{SB} - \Re(\lambda_6))v_H^2, \quad (26)$$

$$M_{12}^2 = M_{21}^2 = -\Im(\kappa^2) - \frac{1}{2}\Im(\lambda_6)v_H^2. \quad (27)$$

Notice that M_{12}^2 is in general nonzero because it is not possible to render κ^2 and λ_6 real by a field phase redefinition of ϕ_B . The mass eigenstates S_1, S_2 are defined through the rotation matrix

$$\begin{pmatrix} \phi_{BR} \\ \phi_{BI} \end{pmatrix} = \begin{pmatrix} \cos \theta & \sin \theta \\ -\sin \theta & \cos \theta \end{pmatrix} \begin{pmatrix} S_1 \\ S_2 \end{pmatrix}, \quad (28)$$

with a mixing angle

$$\sin 2\theta = \frac{2\Im(\kappa^2) + \Im(\lambda_6)v_H^2}{M_{S_1}^2 - M_{S_2}^2}, \quad (29)$$

and masses

$$M_{S_1, S_2}^2 = \frac{1}{2} \left[2\mu_B^2 + \lambda_{SB}v_H^2 \mp \sqrt{[2\Im(\kappa^2) + \Im(\lambda_6)v_H^2]^2 + [2\Re(\kappa^2) + \Re(\lambda_6)v_H^2]^2} \right], \quad (30)$$

where we assumed, without loss of generality, that S_1 is the lightest of the mass eigenstates, $M_{S_1} < M_{S_2}$. Let us stress that the existence of complex parameters in \mathcal{V}_3 is required to have a mixing between ϕ_{BR} and ϕ_{BI} .

From \mathcal{V}_3 , the trilinear interaction between S_1, S_2 and the Higgs boson can be seen to be

$$\mathcal{L} \supset v_H \lambda_6 \sin 2\theta S_1 S_2 h, \quad (31)$$

which implies that, as long as λ_6 and θ are non-zero, S_2 is unstable independently of its mass. In addition, the interaction in equation (31) leads to coannihilation processes between S_1 and S_2 mediated by the Higgs boson (see figure 10). Such processes are absent in Z_{2n+1} models and constitute a novelty of the scenarios in this section.

As a case study, let us extend the $Z_6(13)$ scenario along these lines. Accordingly, the scalar potential \mathcal{V}_2 now reads

$$\mathcal{V}_2^{Z_6}(\phi_1, \phi_3) = \frac{1}{3}\lambda'_{41}\phi_1^3\phi_3 + \frac{1}{3}\lambda'_{42}\phi_1^3\phi_3^* + \text{h.c.} \quad (32)$$

To establish the impact of considering ϕ_3 complex, the magnitude of the relevant quartic free parameters of this scenario are varied between 10^{-4} and 1. The results from the scan are displayed in figure 7 for the $M_{S_1} < M_{\phi_1}$ case (the results for the $M_{\phi_1} < M_{S_1}$ case are the same of those with ϕ_3 real). This case admits $S_1 S_2$ coannihilations, which are quite efficient on depleting Ω_{S_1} and therefore the whole range for M_{S_1} remains valid, with the remarkable fact that Ω_{S_1} can be the subdominant contribution for $M_{S_1} \gtrsim 100$ GeV, reaching even values less than 10% of the total dark matter relic density. The results also indicate that both ϕ_1 and S_1 may be observed at current and forth-coming direct detection experiments, as it is shown in the bottom panels.

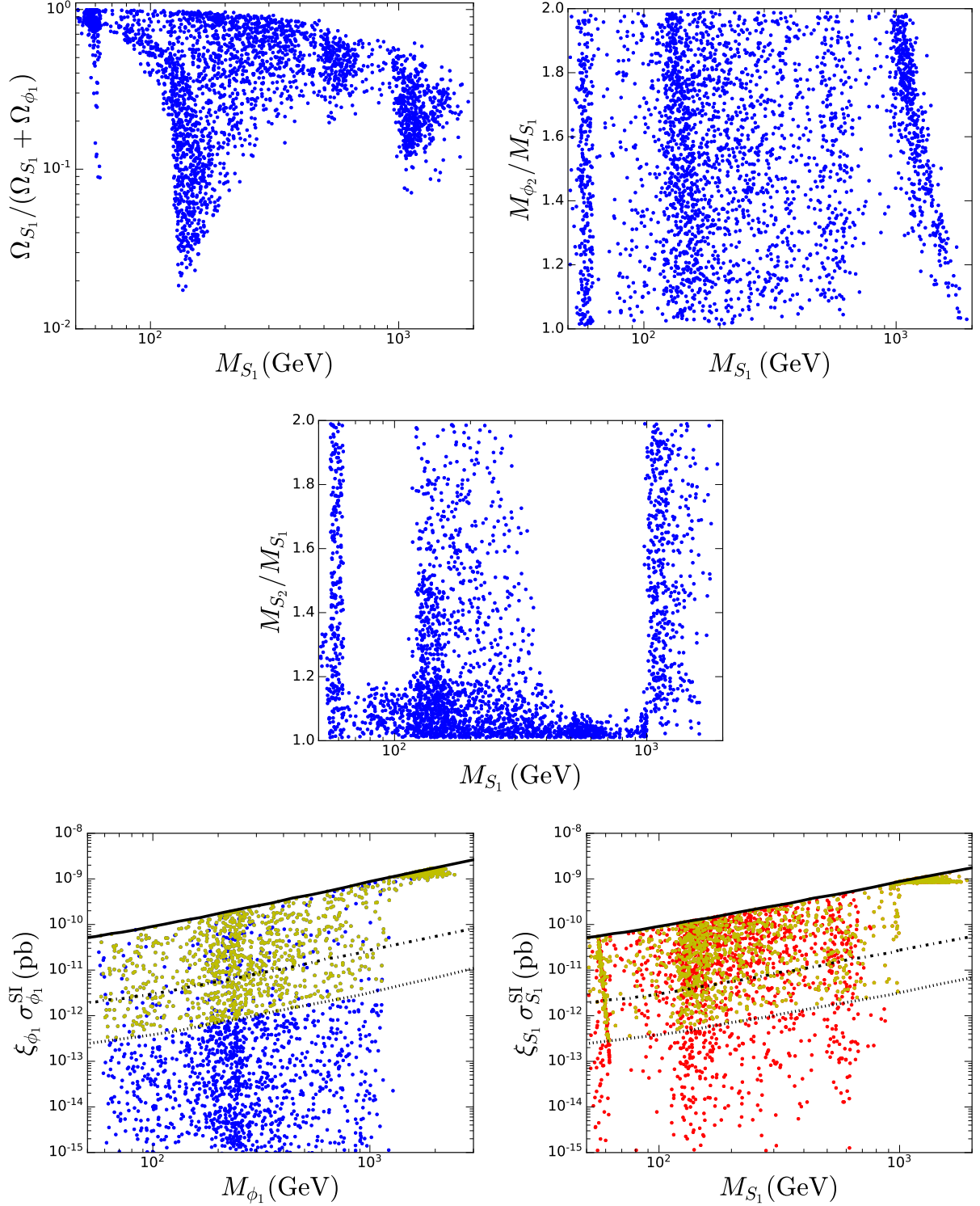


FIG. 11. A sample of viable points of the $Z_6(13)$ model with complex fields and $M_{S_1} < M_{\phi_1}$, projected along different dimensions. The top panels show scatter plots of M_{S_1} versus Ω_{S_1}/Ω_{DM} (left) and versus the ratio of dark matter masses (right). The center panel show the ratio M_{S_2}/M_{S_1} —see text for details. The direct detection prospects are shown in the bottom panels for ϕ_1 (left) and S_1 (right).

It is clear then that by taking ϕ_3 complex rather than real in the $Z_6(13)$ model, new viable regions of parameter space have appeared, and the model has become viable for dark matter masses below 1 TeV. This kind of extension can straightforwardly be applied to other Z_{2n} models.

V. DISCUSSION

The results presented in the previous sections make manifest the fact that the specific interactions associated to each Z_{2n} symmetry (μ_{S_1} , λ'_{41} and μ_{32} for the Z_4 , $Z_6(13)$ and $Z_6(23)$ scenarios, respectively) are crucial in reducing the number density of the lighter dark matter particle. Without them, there would be no new viable regions of parameter space. We can now extrapolate what we have learned about these scenarios to qualitatively discuss the dark matter phenomenology of other Z_{2n} models.

Let us denote the two dark matter particles by ϕ_A (the complex one) with $A < n$ and $\phi_B = \phi_n$ (the real one) with Z_{2n} charges w^A and $w^n = -1$, respectively. For a Z_8 ($n = 4$) symmetry the complete set of possibilities for the two dark matter particles are $A = 1, 2, 3$. For the scenarios (ϕ_1, ϕ_4) and (ϕ_3, ϕ_4) the Z_8 symmetry does not allow any extra invariant term in \mathcal{V}_2 , that is

$$\mathcal{V}_2^{Z_8}(\phi_1, \phi_4) = \mathcal{V}_2^{Z_8}(\phi_3, \phi_4) = 0. \quad (33)$$

Thus we expect, in analogy with the $Z_6(13)$ scenario already discussed, no viable points for $70 \lesssim M_{\phi_1}/\text{GeV} \lesssim 1850$ in the case $M_{\phi_1} < M_{\phi_3}$ and in the range $70 \lesssim M_{\phi_3}/\text{GeV} \lesssim 950$ in the case $M_{\phi_3} < M_{\phi_1}$. The third possibility is the scenario (ϕ_2, ϕ_4) where the Z_8 symmetry allows terms that are equivalent to Eq. (5), that is,

$$\mathcal{V}_2^{Z_8}(\phi_2, \phi_4) = \frac{1}{2} [\mu_{S_2} \phi_2^2 \phi_4 + \lambda_{52} \phi_2^4] + \text{h.c.} \quad (34)$$

Therefore the results obtained for the Z_4 model are the same as for this scenario. And this conclusion can be generalised to all the scenarios based on a Z_{4n} symmetry with dark matter fields ϕ_n and ϕ_{2n} .

Along the same lines, all the scenarios with $n = 5$ feature

$$\mathcal{V}_2^{Z_{10}}(\phi_A, \phi_5) = 0, \quad A = 1, 2, 3, 4, \quad (35)$$

so that again no new viable regions are expected. Scenarios invariant under a Z_{6n} symmetry with dark matter fields ϕ_n and ϕ_{3n} (ϕ_{2n} and ϕ_{3n}) turn out to be equivalent to the $Z_6(13)$ ($Z_6(23)$) scenario we already analyzed. All these results suggest that the Z_4 and Z_6 models studied in this work constitute prototypes for all the Z_{2n} models with one complex and one real fields.

Finally, let us recall that we have identified the parameters that are expected to be relevant for the different models, and have illustrated the generic mechanisms that allow to satisfy the different bounds imposed. In this sense, therefore, this work constitutes a first step towards the elaboration of deep statistical analysis involving different sampling algorithms [46] such as Markov chain Monte Carlo [47] or multimodal nested sampling [48].

VI. CONCLUSIONS

In this paper we considered two-component dark matter scenarios with scalar singlets that transform non-trivially under a Z_{2n} symmetry, where the dark matter consists of a complex field and a real field. We paid particular attention to the $n = 2$ and $n = 3$ cases since they represent the simplest realizations of these scenarios and serve as prototypes for higher Z_{2n} models. We performed a phenomenological analysis of three scenarios based on the Z_4 and Z_6 symmetries, and obtained using a logarithmically-uniform distribution a large sample of points compatible with current bounds. The analysis of this sample shows that, thanks to the semi-annihilations induced by the trilinear interactions, the Z_4 and $Z_6(23)$ scenarios become viable over the entire range of dark matter masses considered, $M \lesssim 2$ TeV, and that they can be probed by future direct detection experiments. In fact, both dark matter particles could be detected in several cases, and, in the $Z_6(23)$ scenario, the observation of one of them at DARWIN is practically guaranteed. The $Z_6(13)$ scenario, on the other hand, is quite constrained because semi-annihilation processes are absent while dark matter conversion processes are inefficient at depleting the abundance of the lightest dark matter particle. Nonetheless, by considering as complex both dark matter fields we showed that it is possible to revert substantially this result. All in all, we demonstrated that this new kind of two-component dark matter models are viable and interesting alternatives to explain one of the greatest mysteries of our time –the nature of the dark matter.

ACKNOWLEDGMENTS

The work of OZ is supported by Sostenibilidad-UdeA and the UdeA/CODI Grants 2017-16286 and 2020-33177.

[1] V. Silveira and A. Zee, *Phys. Lett. B* **161**, 136 (1985).

- [2] J. McDonald, *Phys. Rev.* **D50**, 3637 (1994), [arXiv:hep-ph/0702143 \[HEP-PH\]](#).
- [3] C. Burgess, M. Pospelov, and T. ter Veldhuis, *Nucl. Phys. B* **619**, 709 (2001), [arXiv:hep-ph/0011335](#).
- [4] J. M. Cline, K. Kainulainen, P. Scott, and C. Weniger, *Phys. Rev.* **D88**, 055025 (2013), [Erratum: *Phys. Rev.* D92, no.3, 039906(2015)], [arXiv:1306.4710 \[hep-ph\]](#).
- [5] P. Athron, J. M. Cornell, F. Kahlhoefer, J. McKay, P. Scott, and S. Wild, *Eur. Phys. J. C* **78**, 830 (2018), [arXiv:1806.11281 \[hep-ph\]](#).
- [6] B. Batell, *Phys. Rev.* **D83**, 035006 (2011), [arXiv:1007.0045 \[hep-ph\]](#).
- [7] G. Belanger, K. Kannike, A. Pukhov, and M. Raidal, *JCAP* **1204**, 010 (2012), [arXiv:1202.2962 \[hep-ph\]](#).
- [8] G. Bélanger, K. Kannike, A. Pukhov, and M. Raidal, *JCAP* **1406**, 021 (2014), [arXiv:1403.4960 \[hep-ph\]](#).
- [9] C. E. Yaguna and O. Zapata, *JHEP* **03**, 109 (2020), [arXiv:1911.05515 \[hep-ph\]](#).
- [10] C. Boehm, P. Fayet, and J. Silk, *Phys. Rev.* **D69**, 101302 (2004), [arXiv:hep-ph/0311143 \[hep-ph\]](#).
- [11] E. Ma, *Annales Fond. Broglie* **31**, 285 (2006), [arXiv:hep-ph/0607142 \[hep-ph\]](#).
- [12] Q.-H. Cao, E. Ma, J. Wudka, and C. P. Yuan, (2007), [arXiv:0711.3881 \[hep-ph\]](#).
- [13] T. Hur, H.-S. Lee, and S. Nasri, *Phys. Rev.* **D77**, 015008 (2008), [arXiv:0710.2653 \[hep-ph\]](#).
- [14] H.-S. Lee, *Phys. Lett.* **B663**, 255 (2008), [arXiv:0802.0506 \[hep-ph\]](#).
- [15] K. M. Zurek, *Phys. Rev.* **D79**, 115002 (2009), [arXiv:0811.4429 \[hep-ph\]](#).
- [16] V. Barger, P. Langacker, M. McCaskey, M. Ramsey-Musolf, and G. Shaughnessy, *Phys. Rev. D* **79**, 015018 (2009), [arXiv:0811.0393 \[hep-ph\]](#).
- [17] S. Profumo, K. Sigurdson, and L. Ubaldi, *JCAP* **0912**, 016 (2009), [arXiv:0907.4374 \[hep-ph\]](#).
- [18] G. Belanger and J.-C. Park, *JCAP* **1203**, 038 (2012), [arXiv:1112.4491 \[hep-ph\]](#).
- [19] H. Baer, A. Lessa, S. Rajagopalan, and W. Sreethawong, *JCAP* **1106**, 031 (2011), [arXiv:1103.5413 \[hep-ph\]](#).
- [20] Z.-P. Liu, Y.-L. Wu, and Y.-F. Zhou, *Eur. Phys. J. C* **71**, 1749 (2011), [arXiv:1101.4148 \[hep-ph\]](#).
- [21] I. P. Ivanov and V. Keus, *Phys. Rev.* **D86**, 016004 (2012), [arXiv:1203.3426 \[hep-ph\]](#).
- [22] G. Bélanger, F. Boudjema, A. Pukhov, and A. Semenov, *Comput. Phys. Commun.* **192**, 322 (2015), [arXiv:1407.6129 \[hep-ph\]](#).
- [23] S. Esch, M. Klasen, and C. E. Yaguna, *JHEP* **09**, 108 (2014), [arXiv:1406.0617 \[hep-ph\]](#).
- [24] G. Bélanger, A. Pukhov, C. E. Yaguna, and O. Zapata, *JHEP* **09**, 030 (2020), [arXiv:2006.14922 \[hep-ph\]](#).
- [25] D. S. Akerib *et al.* (LUX-ZEPLIN), *Phys. Rev. D* **101**, 052002 (2020), [arXiv:1802.06039 \[astro-ph.IM\]](#).
- [26] J. Aalbers *et al.* (DARWIN), *JCAP* **1611**, 017 (2016), [arXiv:1606.07001 \[astro-ph.IM\]](#).
- [27] K. P. Modak, D. Majumdar, and S. Rakshit, *JCAP* **03**, 011 (2015), [arXiv:1312.7488 \[hep-ph\]](#).
- [28] A. Biswas, D. Majumdar, and P. Roy, *JHEP* **04**, 065 (2015), [arXiv:1501.02666 \[hep-ph\]](#).
- [29] S. Bhattacharya, P. Poulse, and P. Ghosh, *JCAP* **04**, 043 (2017), [arXiv:1607.08461 \[hep-ph\]](#).

- [30] S. Bhattacharya, P. Ghosh, T. N. Maity, and T. S. Ray, *JHEP* **10**, 088 (2017), [arXiv:1706.04699 \[hep-ph\]](#).
- [31] M. Pandey, D. Majumdar, and K. P. Modak, *JCAP* **06**, 023 (2018), [arXiv:1709.05955 \[hep-ph\]](#).
- [32] J. Hernandez-Sanchez, V. Keus, S. Moretti, D. Rojas-Ciofalo, and D. Sokolowska, (2020), [arXiv:2012.11621 \[hep-ph\]](#).
- [33] B. Patt and F. Wilczek, (2006), [arXiv:hep-ph/0605188 \[hep-ph\]](#).
- [34] G. Arcadi, A. Djouadi, and M. Raidal, *Phys. Rept.* **842**, 1 (2020), [arXiv:1903.03616 \[hep-ph\]](#).
- [35] E. Ma, *Phys. Lett. B* **662**, 49 (2008), [arXiv:0708.3371 \[hep-ph\]](#).
- [36] G. Belanger, K. Kannike, A. Pukhov, and M. Raidal, *JCAP* **01**, 022 (2013), [arXiv:1211.1014 \[hep-ph\]](#).
- [37] A. Hektor, A. Hryczuk, and K. Kannike, *JHEP* **03**, 204 (2019), [arXiv:1901.08074 \[hep-ph\]](#).
- [38] S.-M. Choi, J. Kim, P. Ko, and J. Li, (2021), [arXiv:2103.05956 \[hep-ph\]](#).
- [39] N. Aghanim *et al.* (Planck), *Astron. Astrophys.* **641**, A6 (2020), [arXiv:1807.06209 \[astro-ph.CO\]](#).
- [40] E. Aprile *et al.* (XENON), *Phys. Rev. Lett.* **121**, 111302 (2018), [arXiv:1805.12562 \[astro-ph.CO\]](#).
- [41] A. M. Sirunyan *et al.* (CMS), *Phys. Lett. B* **793**, 520 (2019), [arXiv:1809.05937 \[hep-ex\]](#).
- [42] (2020).
- [43] M. Ackermann *et al.* (Fermi-LAT), *Phys. Rev. Lett.* **115**, 231301 (2015), [arXiv:1503.02641 \[astro-ph.HE\]](#).
- [44] E. Charles *et al.* (Fermi-LAT), *Phys. Rept.* **636**, 1 (2016), [arXiv:1605.02016 \[astro-ph.HE\]](#).
- [45] F. S. Queiroz and C. Siqueira, *JCAP* **04**, 048 (2019), [arXiv:1901.10494 \[hep-ph\]](#).
- [46] G. D. Martinez, J. McKay, B. Farmer, P. Scott, E. Roebber, A. Putze, and J. Conrad (GAMBIT), *Eur. Phys. J. C* **77**, 761 (2017), [arXiv:1705.07959 \[hep-ph\]](#).
- [47] J. Dunkley, M. Bucher, P. G. Ferreira, K. Moodley, and C. Skordis, *Mon. Not. Roy. Astron. Soc.* **356**, 925 (2005), [arXiv:astro-ph/0405462](#).
- [48] F. Feroz, M. P. Hobson, and M. Bridges, *Mon. Not. Roy. Astron. Soc.* **398**, 1601 (2009), [arXiv:0809.3437 \[astro-ph\]](#).